Precision Limits of Tissue Microstructure Characterization by Magnetic Resonance Imaging

Analia Zwick[1,2,*] Dieter Suter[3] Gershon Kurizki,[4] and Gonzalo A. Álvarez[1,2,5,†]

[1]*Centro Atómico Bariloche, CONICET, CNEA,
S. C. de Bariloche, Argentina*
[2]*Departamento de Física Médica, Instituto de Nanociencia y Nanotecnologia, CONICET, CNEA, S. C. de Bariloche, Argentina*
[3]*Fakultät Physik, Technische Universität Dortmund, Dortmund D-44221, Germany*
[4]*Chemical Physics Department, Weizmann Institute of Science, Rehovot, Israel*
[5]*Instituto Balseiro, CNEA, Universidad Nacional de Cuyo, S. C. de Bariloche, Argentina*

Characterization of microstructures in living tissues is one of the keys to diagnosing early stages of pathology and understanding disease mechanisms. However, the extraction of reliable information on biomarkers based on microstructure details is still a challenge, as the size of features that can be resolved with noninvasive magnetic resonance imaging (MRI) is orders of magnitude larger than the relevant structures. Here we derive from quantum information theory the ultimate precision limits for obtaining such details by MRI probing of water-molecule diffusion. We show that currently available MRI pulse sequences can be optimized to attain the ultimate precision limits by choosing control parameters that are uniquely determined by the expected size, the diffusion coefficient, and the spin relaxation time T_2. By attaining the ultimate precision limit per measurement, the number of measurements and the total acquisition time may be drastically reduced compared to the present state of the art. These results are expected to open alternative avenues towards unraveling diagnostic information by quantitative MRI.

I. INTRODUCTION

Information on compartment sizes and geometrical features of microstructures in living tissues is one of the potential keys to diagnosing pathological tissue changes at early stages and understanding organ malfunctioning due to diseases. For example, the biophysical mechanisms of cancer development and treatment are revealed by microstructure details [1–4]. Another case where small structural changes are important indicators are neuronal diseases that alter the distribution of axon diameters and myelin sheath, and thereby the speed of information propagation in the white matter of our brain [5–10]. Such diseases include Alzheimer's disease, autism, amyotrophic lateral sclerosis, and schizophrenia. Therefore, a major goal of medical diagnosis is the development of precise and noninvasive techniques for characterizing the distribution of axon diameters in the brain and, more generally, the size of microstructure compartments in tissues [11–14]. In order to find reliable biomarkers based on quantitative characterization of tissue microstructure, the diagnostic

tools should provide precise measures of tissue structure size of the order of a few micrometers. For this purpose, it is not necessary to obtain micron-scale images of individual tissue compartments, but it is important to measure their *average* sizes at this resolution.

Nanosize sensors based on quantum technologies aim at nanoscale imaging of biological tissues [15–21]. However, such imaging is invasive. By contrast, magnetic resonance imaging (MRI) noninvasively detects nuclear spins inherent in biological tissues, commonly in water molecules. Therefore, MRI is an excellent tool for such studies, since it enables detailed, noninvasive characterization of tissues *in vivo*. Its resolution, in terms of voxel sizes, is typically limited to millimeters in clinical studies, or hundreds of microns in preclinical studies, but can be extended to micrometer scales under specific conditions [22,23]. Furthermore, it also offers the potential to quantify structural details that are orders of magnitude smaller than the size of a voxel by monitoring the distance over which water molecules can travel by diffusion until their motion is restricted by walls that are not directly visible, such as cellular membranes. This approach is often called diffusion-weighted imaging (DWI) [24–27]. The most promising DWI technique employs modulated

---

*analia.zwick@gmail.com
†gonzalo.alvarez@cab.cnea.gov.ar

gradient spin-echo (MGSE) sequences that enable detailed microstructure characterization [14,28–32]. Several works have addressed the estimation of compartment sizes by protocols based on various DWI sequences [30–38]. As pointed out in those works, the main open questions are: what resolution can be ultimately achieved by these experiments and how should the experimental parameters be adapted to approach this ultimate limit?

In this work, we provide answers to these important questions by adapting results from quantum-information theory. The ultimate limit is fundamentally determined by quantum mechanics, as the nuclear spins of the diffusing molecules are the microstructure sensors. Therefore, we analytically obtain the limiting resolution for the important case where the size of tissue microstructures is probed by diffusion processes via DWI experiments. We derive the necessary control conditions for MGSE sequences to allow the attainment of this limit. As examples, we consider sequences with typical modulated gradient waveforms for the estimation of microstructure compartment sizes, assuming generic geometries. We show that the ultimate precision limit of the estimation is achievable by MGSE sequences if the gradient strength is set to a value that depends on the microstructure size, the T_2 relaxation time, and the diffusion coefficient of the molecules within the compartments. Based on this result, an optimization protocol is provided for MGSE sequences capable of attaining the highest possible precision under the given experimental constraints. With this protocol, the total acquisition time of quantitative microstructure imaging is shown to be *drastically reduced*, taking into account the limitations of the available hardware and the microscopic properties of the tissues being studied, such as diffusion constants and spin relaxation times.

II. DIFFUSION-WEIGHTED SPIN-ECHO NMR SIGNAL

Nuclear spins of molecules in biological tissues, in particular the spins $s = \frac{1}{2}$ of protons in water molecules, interact with external magnetic fields in MRI. A uniform magnetic field along the z axis defines the Larmor precession frequency of the spins. In DWI, uniform magnetic field gradients $G\hat{r}$ are applied along an arbitrary direction $\hat{r}$. The diffusive molecular motion of the spins is therefore reflected in a fluctuating precession frequency $\omega(t) = \gamma\vec{G}\cdot\vec{r}(t)$, where $\vec{r}(t)$ is the instantaneous position of the diffusing spin and γ is the gyromagnetic factor of the nucleus [26,27]. If the motion of the molecules is restricted, e.g., due to compartmentalization of the tissue, such as in the human brain, the fluctuations are limited in amplitude. Quantification of these fluctuations therefore allows one to obtain an indirect measure of the size distribution of these compartments [11–14].
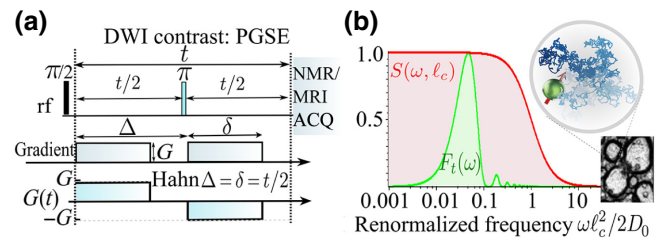

FIG. 1. Diffusion-weighted spin-echo probing of molecular diffusion. (a) Pulsed gradient spin-echo (PGSE) sequence: an initial $\pi/2$-excitation pulse is followed by the diffusion-weighting contrast block consisting of a π rf pulse at half the evolution time t between two-pulsed gradients of duration δ separated by a delay Δ. The π pulse refocuses external magnetic field inhomogeneities and modulates the effective gradient $G(t)$, switching its sign as shown in the bottom of the scheme. The remaining signal is measured using MRI encoding during the acquisition time (ACQ). (b) Normalized displacement power spectrum $S(\ell_c, \omega)$ of the restricted molecular diffusion (inset schematic) and a suitable MGSE filter function $F_t(\omega)$ as a function of the renormalized frequency $\omega\ell_c^2/2D_0$. The PGSE filter assumes that $\delta = \Delta = t/2$.

A typical MRI or DWI experiment starts with a $\pi/2$-excitation pulse, which creates a coherent superposition of the two spin states. During the subsequent evolution time t, the magnetization evolves and records the diffusion process. The simplest MGSE sequence is the so-called PGSE sequence [24] [Fig. 1(a)]. Within the evolution time t, two gradient pulses of duration δ are applied with a delay Δ between them. The PGSE sequence includes one π rf pulse to refocus external magnetic field inhomogeneities and switch the effective gradient sign $G(t)$ to refocus the spin's dephasing evolution during the gradients. After this evolution, the total magnetization is encoded spatially by a MRI sequence at the end of this evolution.

We consider here that $M(t)$ is the magnetization in a voxel of the image, which provides what is called the diffusion-weighted contrast generated by the MGSE sequence. A Gaussian phase distribution is typically assumed for the random phase $\phi(t)$ accumulated by the spins, leading, under probing by a MGSE sequence, to a decay of the magnetization [39]

$$M(t) = e^{-\langle\phi^2(t)\rangle/2}M(0), \tag{1}$$

where the angular brackets represent the ensemble average over the random phases. Here, the signal attenuation $e^{-\langle\phi^2(t)\rangle/2}$ accounts for the contrast generated in an image, based on the effect of the MGSE sequence that probes different time scales of the diffusion process. Depending on how the spins are scrambled by the diffusion process, the refocusing efficiency varies and is manifested in the signal attenuation. The phase variance can be described in the frequency domain by the following expression [29,40–42], which is the example for the case of phase diffusion

of the Kofman-Kurizki universal formula for decoherence (dephasing and relaxation) control, and probing in quantum systems [42–48]:

$$\langle \phi^2(t) \rangle = \gamma^2 \int_{-\infty}^{\infty} d\omega F_t(\omega) S(\omega). \quad (2)$$

The phase variance is a convolution of two spectral functions. (i) The filter function $F_t(\omega) = (1/2\pi)$ $|\int_0^t dt' G(t') e^{-i\omega t'}|^2$ is the finite-time Fourier transform (FT) of the effective magnetic field gradient $G(t)$ modulated with MGSE sequences, either directly or by applying π rf pulses. Here $F_t(\omega)$ acts as a spectral noise filter: if its value is 1, it passes the experimental noise at that frequency without attenuation, whereas if it is 0, it blocks the noise completely. (ii) The spectral density $S(\omega)$ of the spin noise induced by the environment is given (in the case of diffusion) by the FT of the molecule displacement autocorrelation function $\langle \Delta r(t) \Delta r(t + \tau) \rangle$, where $\Delta r(t) = r(t) - \langle r(t) \rangle$ is the instantaneous position deviation from its average value [40,41]. For the case of restricted diffusion, $\langle \Delta r(t) \Delta r(t + \tau) \rangle = D_0 \tau_c e^{-|\tau|/\tau_c}$, where D_0 is the free diffusion coefficient [30,35,49] and τ_c is the correlation time. For molecules that diffuse in a microstructure, the characteristic time τ_c is that required on average for a molecule to probe the boundaries of the compartment characterized by the restriction length ℓ_c. It is related to the restriction length by Einstein's expression $\ell_c^2 = 2D_0 \tau_c$ [27]. The Fourier transform of the autocorrelation function, the displacement spectral density $S(\omega)$, is given by [28,30,35,41,48]

$$S(\omega) = \frac{D_0 \tau_c^2}{\pi(1 + \omega^2 \tau_c^2)}. \quad (3)$$

In Fig. 1(b) we show the filter function $F_t(\omega)$ for the PGSE sequence, superimposed over the spectral density $S(\omega)$.

In restricted diffusion, the restriction length ℓ_c and the geometric size of the compartment depend on its shape (Appendix A). For the example of cylinders oriented perpendicular to the direction of the magnetic field gradient, a good approximation is $\ell_c = 0.37d$, where d is the cylinder diameter [28,30,35,40].

III. ULTIMATE ERROR BOUNDS FOR ESTIMATING MICROSTRUCTURE SIZES

The central question we pose is: what is the best MGSE control strategy to infer the restriction length of the diffusion process? This limit is dictated by quantum mechanics and we therefore use tools developed in quantum information.

The figure of merit for the estimation of ℓ_c, the parameter that determines microstructure sizes, is the relative error $\delta\ell_c/\ell_c$. Assuming unbiased single-parameter estimation,

the relative error of the magnetization signal in Eq. (1) is limited by the quantum Cramer-Rao bound ε_{CR}, where

$$\frac{\delta\ell_c}{\ell_c} \geq \frac{\varepsilon_{CR}(t, \ell_c)}{\sqrt{\mathcal{N}}} = \frac{1}{\ell_c \sqrt{\mathcal{N} \mathcal{F}_Q(t, \ell_c)}}, \quad (4)$$

i.e., ε_{CR} *is the minimal attainable relative error per measurement*, which is determined by the quantum Fisher information (QFI) $\mathcal{F}_Q(t, \ell_c)$ of ℓ_c obtainable from the measured magnetization for a given MGSE sequence and $\mathcal{N}$ is the number of measurements [50,51]. The QFI depends on the magnetization signal in Eq. (1) [48,50,52,53] with a functional dependence on ℓ_c and the total diffusion-weighting time t:

$$\mathcal{F}_Q(t, \ell_c) = \frac{[M(t, \ell_c)/M(0)]^2}{1 - [M(t, \ell_c)/M(0)]^2} \left(\frac{\partial \ln[M(t, \ell_c)/M(0)]}{\partial \ell_c} \right)^2. \quad (5)$$

This expression implicitly depends on other MGSE control and system parameters, particularly the diffusion coefficient D_0 that we assume to be known. By maximizing $\mathcal{F}_Q$ with respect to the evolution time t for a given MGSE control, ε_{CR} is minimized [48]. Therefore, the optimal evolution time t_{opt} defined by $\mathcal{F}_Q(t_{opt}, \ell_c) = \max_t[\mathcal{F}_Q(t, \ell_c)]$ provides the minimum error for a given MGSE sequence

$$\varepsilon = \varepsilon_{CR}(t_{opt}, \ell_c), \quad (6)$$

based on achieving the best trade-off between the amplitude contrast of the diffusion-weighted echo signal $[M^2(t, \ell_c)\{M^2(0) - M^2(t, \ell_c)\}^{-1}]$ and its parametric sensitivity to ℓ_c, $|\partial \ln[M(t, \ell_c)/M(0)]/\partial \ell_c|^2$ according to Eq. (5). Then, by considering *all* possible MGSE sequences we demonstrate (Appendix B) that this error is lower bounded by

$$\varepsilon \geq \varepsilon_0 = \min_{\{MGSE\}} \varepsilon \approx 0.62. \quad (7)$$

This ultimate precision estimation bound ε_0 for ℓ_c is *general* for all possible MGSE control sequences and remarkably, *independent* of the particular geometry restricting the diffusion (Appendix A). We can see that, by suitably designing an optimal MGSE control sequence, we can attain this ultimate relative-error bound ε_0 for the restriction length of the diffusion process.

IV. ATTAINING THE ULTIMATE PRECISION BOUND

To attain the ultimate error bound per measurement in Eq. (7), we need to optimally choose the relation between

the length scales

$$\ell_G = \sqrt[3]{\frac{2D_0}{\gamma G}}, \qquad \ell_c = \sqrt{2D_0\tau_c}, \qquad \ell_D = \sqrt{2D_0 t}, \quad (8)$$

where ℓ_G is the dephasing length, ℓ_c is the restriction length, and ℓ_D is the diffusion length. The MGSE control sequence should satisfy the following requirements. (i) The spectral filter $F_t(\omega)$ should only overlap with the displacement power spectrum $S(\ell_c, \omega)$ [Eq. (3)] within the spectral region of the strongest dependence on ℓ_c to enhance the estimation sensitivity. This regime here is attained at a *low frequency*, where $S(\ell_c, \omega \approx 0) \propto \ell_c^4$, corresponding to $-\ln[M(t)/M(0)] \propto \ell_c^4$. (ii) The total evolution time t should be the optimal time t_{opt}, Eq. (6), such that $\ln[M(t_{\text{opt}}, \ell_c)/M(0)] = \ln M_o \approx 0.8$, where the best trade-off between the parametric sensitivity and an optimal magnetization contrast M_o is obtained as derived in Appendix B. A MGSE sequence producing a narrow *low-frequency* bandpass filter therefore defines the experiment that is most sensitive to the restriction size ℓ_c. The narrowest low-frequency bandpass filter for a given evolution time among typical MGSE sequences is an optimized PGSE sequence, as it only contains one gradient sign switch leading to the longest possible modulation period. The optimized PGSE is analogous to a Hahn spin echo with a constant gradient when $\delta = \Delta = t/2$ [Fig. 1(a)], and produces the lowest frequency bandpass under this limit (Appendix C).

If $t \gg \tau_c$, condition (i) is satisfied (Appendix C). From requirements (i)–(ii), the optimal evolution time is

$$t_{\text{opt}} = \frac{-\ln M_o}{\gamma^2 G^2 D_0 \tau_c^2} \approx \frac{0.8}{\gamma^2 G^2 D_0 \tau_c^2}. \quad (9)$$

In Fig. 2(a) we show typical signal decay for different $\gamma^2 G^2 D_0 \tau_c^3$ values and the corresponding optimal evolution times t_{opt}. Both requirements (i) and (ii) are therefore fulfilled when $t = t_{\text{opt}} \gg \tau_c$, meaning that the diffusion length should be large compared to the restriction length, $\ell_D \gg \ell_c$ (Eq. 8). Together with Eq. (9), this requirement amounts to the condition $\gamma^2 G^2 D_0 \tau_c^3 \ll 1$, which means that the diffusion restriction length should be much smaller than the dephasing length, $\ell_c \ll \ell_G$. Indeed, the optimal ratio between the diffusion-weighted and dephasing lengths ℓ_D/ℓ_G, which yields the highest precision for the restriction length, is seen from Fig. 2(b) to require

$$\frac{\ell_c^6}{\ell_G^6} = \gamma^2 G^2 D_0 \tau_c^3 \ll 1. \quad (10)$$

Therefore, under the idealized relaxation-free condition discussed here, *increasing ℓ_G*, i.e., reducing the gradient strength, *always improves the precision* up to the
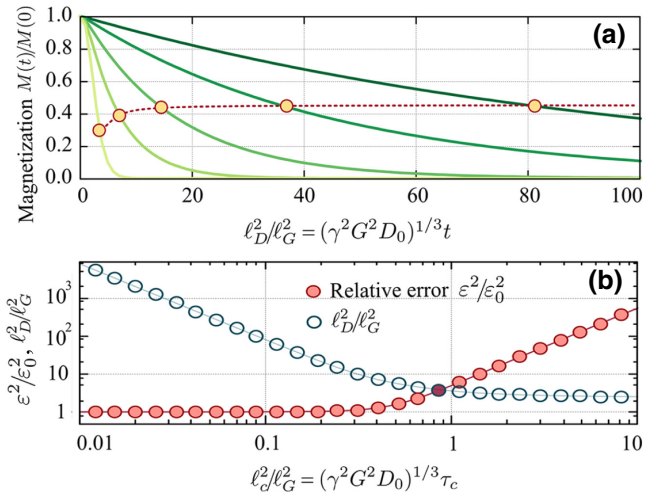

FIG. 2. Attaining the ultimate precision bound of the restriction length ℓ_c from diffusion-weighted magnetization decay. (a) Magnetization decay $M(t)/M(0)$ under Hahn MGSE control as a function of the evolution time in units of the ratio between the diffusion and dephasing lengths ℓ_D^2/ℓ_G^2. Dark to light green lines denote increasing renormalized correlation times in units of the ratio between the restriction and dephasing lengths $\ell_c^2/\ell_G^2 = (\gamma^2 G^2 D_0)^{1/3} \tau_c = 0.1, 0.15, 0.25, 0.4, 1$. The circles denote the optimal evolution times $(\gamma^2 G^2 D_0)^{1/3} t_{\text{opt}}$. (b) Red circles show the relative minimum error $\varepsilon^2/\varepsilon_0^2$ in the estimation of ℓ_c as a function of ℓ_c^2/ℓ_G^2 that yields the number of measurements $\mathcal{N}$ needed to attain the ultimate precision bound per measurement. Blue circles show the corresponding value of ℓ_D^2/ℓ_G^2 as a function of ℓ_c^2/ℓ_G^2. The bound is approached when $\ell_c^2/\ell_G^2 \ll 1$ and $\ell_D^2/\ell_G^2 \gg 1$, and $(\ell_c^4/\ell_G^4)(\ell_D^2/\ell_G^2) = -\ln M_0$ as described in Eq. (9), implying that $(\gamma^2 G^2 D_0)^{1/3} \tau_c \ll 1$.

point that allows us to approach the bound [Eq. (7)]. Since the optimal time must fulfill Eq. (9), it must satisfy the condition $t_{\text{opt}}/\tau_c = (\ell_D^2/\ell_G^2)(\ell_G^2/\ell_c^2) \approx (\ell_G^6/\ell_c^6) = (\gamma^2 G^2 D_0 \tau_c^3)^{-1} \gg 1$. By contrast, when $t_{\text{opt}}/\tau_c \lesssim 1$, t_{opt} saturates at a value of the evolution time for which the signal decays below $M/M(0) \approx 1/e$ [Fig. 2(a)]. The larger τ_c, the shorter t_{opt} in Eq. (9), and condition (i) can no longer be satisfied.

In Fig. 2(b) we show the minimal relative squared error per measurement ε^2 scaled to ε_0^2, $\varepsilon^2/\varepsilon_0^2$. This scaled squared error determines the number of measurements $\mathcal{N}$ needed to attain an error equivalent to the ultimate precision per measurement [see Eq. (4)]. For $\ell_c/\ell_G \gtrsim 1$, the restricted diffusion regime is no longer achieved and the relative error increases quadratically with ℓ_c/ℓ_G.

V. PRECISION BOUNDS WITH TRANSVERSE RELAXATION

Under the idealized relaxation-free conditions discussed so far, by reducing the gradient we may always increase the optimal evolution time so as to approach the ultimate precision bound for ℓ_c estimation. In practice, however,

this is limited by the intrinsic dephasing of the nuclear spin (T_2 relaxation) that contributes to the signal decay, independent of the MGSE sequence and the corresponding diffusion weighting. The echo signal of Eq. (1) is then $M_{T_2}(t, \ell_c) = e^{-t/T_2} M(t, \ell_c)$, where $M(t, \ell_c)$ is the diffusion-weighted magnetization of Eq. (1). The relative error including the T_2-relaxation effects is bounded by

$$\varepsilon \geq e^{t/T_2} \varepsilon_0, \tag{11}$$

and thus exponentially increases with t/T_2 (Appendix B).

The conditions for approaching the ultimate error bound ε_0 are now more restrictive, since an evolution time t longer than T_2 causes signal loss that limits the estimation efficiency (Appendix B). The condition $t \ll T_2$ implies specific values for the optimal evolution time t_{opt} and the efficiency parameter $\gamma^2 G^2 D_0 \tau_c^3$ required to approach the ultimate precision limit ε_0, as shown in Fig. 3(a). This is in contrast to the case in which $T_2 \to \infty$, where a semi-infinite range of t_{opt} values exists for $\gamma^2 G^2 D_0 \tau_c^3 \ll 1$ that allow the ultimate error bound to be approached (see Fig. 2).

For a finite value of T_2, we still find a *finite region* where $\varepsilon \approx \varepsilon_0$ when $t_{\text{opt}} \ll T_2$ ($\ell_D \ll \ell_{T_2} = \sqrt{2D_0 T_2}$), as $e^{t/T_2} \approx 1 + \mathcal{O}(t_{\text{opt}}/T_2)$ in Eq. (11). This region is defined by the condition $\ell_c^6/\ell_G^6 \ll 1$, Eq. (10), which has been imposed

to satisfy the requirements for reaching the ultimate error bound. These two conditions imply that the ultimate error bound can be approached only if $\ell_G/\ell_{T_2} \ll 1$. Therefore, the range of restriction lengths ℓ_c that can be determined efficiently with DWI must obey

$$\sqrt{\frac{2D_0}{\gamma^2 G^2 T_2}} \ll \ell_c^2 \ll \left(\frac{2D_0}{\gamma G}\right)^{2/3}, \tag{12}$$

which are limited by the achievable gradient strengths and the T_2-relaxation time. For a given ℓ_c, these conditions define the optimal gradients for estimating ℓ_c:

$$\frac{1}{\gamma \ell_c^2} \sqrt{\frac{2D_0}{T_2}} \ll G \ll \frac{2D_0}{\gamma \ell_c^3}. \tag{13}$$

The minimum relative error for different values of G and ℓ_c is shown in Fig. 3(b), highlighting the optimal values of G for estimating the allowed range of restriction lengths.

VI. CONCLUSIONS

Precise measurements of the size of microscopic tissue compartments, such as the diameter of neuronal axons, are part of an ongoing endeavor to provide improved diagnostic value for many medical conditions. Diffusion of water molecules is an inherent quantum probe of tissue compartment sizes; the molecular motion can be tracked by diffusion-weighted magnetic resonance imaging to access the restriction length of the diffusion process. The present analysis uses tools developed in quantum information science to derive from first principles a universal, ultimate precision limit for estimating microstructure sizes by DWI. This limit is attainable by current MRI techniques available in many clinical settings, provided the relevant control parameters are properly chosen. We show how the optimal control parameters depend on the diffusion coefficient of the probe molecules (typically water), the relaxation time T_2, and the expected restriction length. The results of the present analysis are very encouraging as they show that optimal estimation of microstructure detail, e.g., axon diameters (approximately 0.1–20 μm) is achievable by present technologies, given that modern clinical instruments can apply gradients of T/m [54], and a preclinical microimaging magnet can apply tens of T/m. Even submicron structures can, in principle, be determined with high precision, but this may demand higher field gradients that are currently unavailable in clinical magnets. While an extension of this work needs to be performed to account for multiparameter estimation as in biological tissues there always exist heterogeneity, our results still provide the fundamental estimation limits for each individual compartment size. In particular, in several biological tissue regions, microstructure sizes can be described with a log-normal
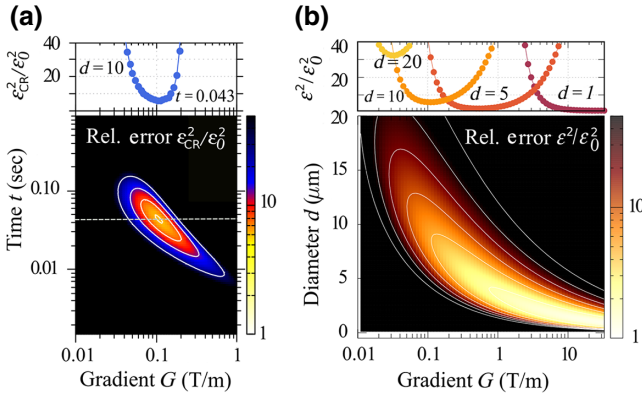
FIG. 3. Optimal control parameters for the estimation of the restriction length ℓ_c. We consider the PGSE sequence with $\Delta = \delta$ (Hahn) and typical diffusion coefficient $D_0 = 1 \times 10^{-5}$ cm²/s and relaxation time $T_2 = 0.1$ s for the brain's gray-white matter. (a) Normalized Cramer-Rao error $\varepsilon_{\text{CR}}^2/\varepsilon_0^2$ in the estimation of ℓ_c as a function of time and gradient strength G for a cylindrical compartment with diameter $d = 10$ μm ($\ell_c = 0.37d$), typical for axons or microfibers. The top inset shows $\varepsilon_{\text{CR}}^2/\varepsilon_0^2$ versus G for an evolution time $t = 43$ ms, shown by the white dashed line in the main panel. (b) The normalized relative error $\varepsilon^2/\varepsilon_0^2$ as a function of G and diameter d. The top inset shows $\varepsilon^2/\varepsilon_0^2$ for $d = 1, 5, 10, 20$ μm. The number of measurements required to attain ε_0 under the optimal conditions grows as the diameter d increases or T_2 decreases. Equivalently, the range of optimal G values that approximate ε_0 is reduced as $\tau_c = \frac{1}{2}\ell_c^2/D_0$ approaches T_2 (Eq. 13).

distribution, as in the Corpus Callosum [8,11,13,38,55–57]. Here, a two-parameter estimation procedure should be implemented for an optimal information gain (e.g., width and median size of the distribution). However, regions with narrow distributions are well represented with a unique size. The present results advance us towards designing quantitative and precise imaging approaches that open alternative avenues for characterizing tissue microstructures in the shortest time possible, which is imperative for finding useful biomarkers for medical diagnosis. These fundamental limits of parameter-estimation optimization can also be exploited for developing nanosize quantum sensors based on noise spectroscopy that can be injected into biological tissues [15–19].

APPENDIX A: ESTIMATING RESTRICTION LENGTHS IN GENERAL GEOMETRIES

The spectral density $S(\omega)$ is the Fourier transform of the diffusion correlation function derived from the solution to the Einstein-Fick diffusion equation for a corresponding restricting geometry [28,39–41]. The spectral density is therefore given by

$$S(\omega) = \sum_k \frac{D_0 b_k \tau_k^2}{\pi(1 + \omega^2 \tau_k^2)}, \qquad (A1)$$

where the coefficients b_k and correlation times τ_k depend on the geometry of the compartments and can be found in Ref. [28] for cylinders, spheres, and planar layers. When the MGSE filter overlaps with the displacement power spectrum $S(\omega)$ within the spectral region of low frequency, $S(\ell_c, \omega \approx 0) = \sum_k (D_0 b_k \tau_k^2/\pi) \propto \ell_c^4$. Here the restriction length is determined by the root mean squared correlation time $\ell_c^2 = 2D_0 \sqrt{\sum_k b_k \tau_k^2}$.

Remarkably, the precision estimation bound for ℓ_c, Eq. (7), is general for all possible MGSE control sequences and *independent of the particular geometry* restricting the diffusion.

APPENDIX B: ULTIMATE ERROR BOUND ON ℓ_c

The QFI of ℓ_c for a nuclear spin state under pure dephasing is given by Eq. (5), where the magnetization

M is measured by the spin operator $\langle \sigma_x \rangle$ in the rotating frame precessing at the nuclear spin's Larmor frequency [48,50,52,53]. The magnetization has explicit functional dependence on ℓ_c and the total evolution time t, but implicitly depends on the diffusion coefficient D_0 that we assume to be known, determined by monitoring the free diffusion time scale. Here, the measurement of the observable σ_x is said to be optimal because the QFI coincides with its classical counterpart [48,50,52,53].

The QFI is maximized at t_{opt}, which provides the best trade-off between the amplitude contrast of the diffusion-weighted echo signal $[M^2\{M^2(0) - M^2\}^{-1}]$ and its parametric sensitivity to ℓ_c, $|\partial \ln[M/M(0)]/\partial \ell_c|^2$ [Eq. (5)]. This parametric sensitivity depends on $\partial S/\partial \ell_c$ since the restriction length ℓ_c only appears in the displacement power spectrum, Eq. (3). It is bounded by $|\partial S/\partial \ell_c| \leq 4S/\ell_c$. This bound is only reached when low frequencies are probed by the MGSE filter function. The spectrum in Eq. (3) then becomes a homogeneous function of ℓ_c of order 4, i.e., $S(\ell_c, \omega \approx 0) \propto \ell_c^4$. This dependence leads to the bound

$$\left| \frac{\partial \ln[M/M(0)]}{\partial \ell_c} \right| \leq \frac{4\{-\ln[M/M(0)]\}}{\ell_c}, \qquad (B1)$$

which is attained when the MGSE control is such that it generates a narrow low-frequency bandpass filter. This analysis determines a tight lower bound for the relative error in Eq. (4),

$$\varepsilon_{\text{CR}}(t, \ell_c) \geq \frac{\sqrt{[M(0)]^2 - [M(t, \ell_c)]^2}}{4\{-\ln[M(t, \ell_c)/M(0)]\}M(t, \ell_c)}, \qquad (B2)$$

which is minimized when the condition

$$-\ln\left[\frac{M(t, \ell_c)}{M(0)}\right] = -\ln M_o = 1 + \frac{W(-2e^{-2})}{2} \approx 0.8 \qquad (B3)$$

is fulfilled, with $W(z)$ being the Lambert function. This demonstrate the existence of an *attainable ultimate relative-error bound* for the restriction length of the diffusion process

$$\varepsilon_{\text{CR}}(t, \ell_c) \geq \frac{\sqrt{1 - M_o^2}}{4(-\ln M_o)M_o} = \varepsilon_0 \approx 0.62, \qquad (B4)$$

where $\varepsilon_0 = \{-\frac{1}{2}W(-2e^{-2})[1 + \frac{1}{2}W(-2e^{-2})]\}^{-1/2}/4 \approx 2.48/4 \approx 0.62$.

The T_2 attenuation factor e^{-t/T_2} of the signal decay introduces a crucial constraint for attaining the optimal evolution time that leads to the ultimate precision bound of Eq. (7) in the estimation of ℓ_c. The relative error is now

bounded by

$$\varepsilon_{CR} \geq \frac{e^{t/T_2}\sqrt{M^2(0) - e^{-2t/T_2}M^2}}{4\{-\ln[M/M(0)]\}M} \geq \frac{e^{t/T_2}\sqrt{M^2(0) - M^2}}{4\{-\ln[M/M(0)]\}M}, \tag{B5}$$

which leads to Eq. (11).

APPENDIX C: OPTIMIZED PGSE: HAHN SPIN-ECHO FILTER

The narrowest low-frequency bandpass filter from typical MGSE sequences is an optimized version of the PGSE sequence, as it contains only one gradient sign switch, producing the lowest frequency bandpass. The frequency filter of the PGSE sequence is

$$F_{\delta,\Delta}^{PGSE}(\omega) = \left| \frac{4ie^{-i\omega(\delta+\Delta)/2}\sin(\omega\delta/2)\sin(\omega\Delta/2)}{\omega} \right|^2. \tag{C1}$$

For $\delta = \Delta = t/2$, which corresponds to the well-known gradient or Hahn spin-echo refocusing sequences over the total evolution time t (Fig. 1), the magnetization signal is [28,35,49]

$$M_{\delta=t/2,\Delta=t/2} = e^{-\gamma^2 G^2 D\tau_c^2 t[1-(t/\tau_c)(3+e^{-t/\tau_c}-4e^{-t/2\tau_c})]}M(0). \tag{C2}$$

Under this condition, the sequence produces a low-frequency narrow bandpass filter if $t \gg \tau_c$, resulting in

$$-\ln\left(\frac{M_{\delta=\Delta=t/2,t\gg\tau_c}(t,\ell_c)}{M(0)}\right) \approx \gamma^2 G^2 D_0 \tau_c^2 t \propto \ell_c^4. \tag{C3}$$

---

[1] D. M. Patterson, A. R. Padhani, and D. J. Collins, Technology insight: Water diffusion MRI—a potential new biomarker of response to cancer therapy, Nat. Rev. Clin. Oncol. **5**, 220 (2008).

[2] A. R. Padhani, G. Liu, D. M. Koh, T. L. Chenevert, H. C. Thoeny, T. Takahara, A. Dzik-Jurasz, B. D. Ross, M. Van Cauteren, D. Collins, D. A. Hammoud, G. J. S. Rustin, B. Taouli, and P. L. Choyke, Diffusion-weighted magnetic resonance imaging as a cancer biomarker: Consensus and recommendations, Neoplasia **11**, 102 (2009).

[3] N. S. White *et al.*, Diffusion-weighted imaging in cancer: Physical foundations and applications of restriction spectrum imaging, Cancer Res. **74**, 4638 (2014).

[4] C. Enzinger, F. Barkhof, O. Ciccarelli, M. Filippi, L. Kappos, M. A. Rocca, S. Ropele, À. Rovira, T. Schneider, N. de Stefano, H. Vrenken, C. Wheeler-Kingshott, J. Wuerfel, and F. Fazekas, Nonconventional MRI and microstructural cerebral changes in multiple sclerosis, Nat. Rev. Neurol. **11**, 676 (2015).

[5] J. B. Hursh, Conduction velocity and diameter of nerve fibers, Am. J. Physiol. **127**, 131 (1939).

[6] S. G. Waxman and M. V. L. Bennett, Relative conduction velocities of small myelinated and non-myelinated fibres in the central nervous system, Nat. New Biol. **238**, 217 (1972).

[7] V. Drago *et al.*, Disease tracking markers for alzheimer's disease at the prodromal (MCI) stage, J. Alzheimers Dis. **26**, 159 (2011).

[8] N. S. White, T. B. Leergaard, H. D'Arceuil, J. G. Bjaalie, and A. M. Dale, Probing tissue microstructure with restriction spectrum imaging: Histological and theoretical validation, Hum. Brain Mapp. **34**, 327 (2013).

[9] J. Xu, H. Li, K. D. Harkins, X. Jiang, J. Xie, H. Kang, M. D. Does, and J. C. Gore, Mapping mean axon diameter and axonal volume fraction by MRI using temporal diffusion spectroscopy, Neuroimage **103**, 10 (2014).

[10] F. Grussu, T. Schneider, C. Tur, R. L. Yates, M. Tachrount, A. Ianuş, M. C. Yiannakas, J. Newcombe, H. Zhang, D. C. Alexander, G. C. DeLuca, and C. A. M. Gandini Wheeler-Kingshott, Neurite dispersion: A new marker of multiple sclerosis spinal cord pathology? Ann. Clin. Transl. Neurol. **4**, 663 (2017).

[11] Y. Assaf, T. Blumenfeld-Katzir, Y. Yovel, and P. J. Basser, Axcaliber: A method for measuring axon diameter distribution from diffusion MRI, Magn. Reson. Med. **59**, 1347 (2008).

[12] D. C. Alexander, P. L. Hubbard, M. G. Hall, E. A. Moore, M. Ptito, G. J. Parker, and T. B. Dyrby, Orientationally invariant indices of axon diameter and density from diffusion MRI, Neuroimage **52**, 1374 (2010).

[13] N. Shemesh, G. A. Álvarez, and L. Frydman, Size distribution imaging by non-uniform oscillating-gradient spin echo (NOGSE) MRI, PLoS ONE **10**, e0133201 (2015).

[14] D. S. Novikov, E. Fieremans, S. N. Jespersen, and V. G. Kiselev, Quantifying brain microstructure with diffusion MRI: Theory and parameter estimation, NMR Biomed. **32**, e3998 (2019).

[15] T. Staudacher, N. Raatz, S. Pezzagna, J. Meijer, F. Reinhard, C. A. Meriles, and J. Wrachtrup, Probing molecular dynamics at the nanoscale via an individual paramagnetic centre, Nat. Commun. **6**, 8527 (2015).

[16] P. Wang, S. Chen, M. Guo, S. Peng, M. Wang, M. Chen, W. Ma, R. Zhang, J. Su, X. Rong, F. Shi, T. Xu, and J. Du, Nanoscale magnetic imaging of ferritins in a single cell, Sci. Adv. **5**, eaau8038 (2019).

[17] K. Mouloudakis, M. Loulakis, and I. K. Kominis, Quantum trajectories in spin-exchange collisions reveal the nature of spin-noise correlations in multispecies alkali-metal vapors, Phys. Rev. Res. **1**, 033017 (2019).

[18] E. Moreva, The biosensing with nv centers in diamond: Related challenges, Int. J. Quantum Inf. **18**, 1941023 (2020).

[19] J. F. Barry, M. J. Turner, J. M. Schloss, D. R. Glenn, Y. Song, M. D. Lukin, H. Park, and R. L. Walsworth, Optical magnetic detection of single-neuron action potentials using quantum defects in diamond, Proc. Natl. Acad. Sci. **113**, 14133 (2016).

[20] R. Tenne, U. Rossman, B. Rephael, Y. Israel, A. Krupinski-Ptaszek, R. Lapkiewicz, Y. Silberberg, and D. Oron,

Super-resolution enhancement by quantum image scanning microscopy, Nat. Photonics **13**, 116 (2019).

[21] D. R. Glenn, K. Lee, H. Park, R. Weissleder, A. Yacoby, M. D. Lukin, H. Lee, R. L. Walsworth, and C. B. Connolly, Single-cell magnetic imaging using a quantum diamond microscope, Nat. Methods **12**, 736 (2015).

[22] J. Lambert, R. Hergenröder, D. Suter, and V. Deckert, Probing liquid-liquid interfaces with spatially resolved NMR spectroscopy, Angew. Chem. Int. Ed. **48**, 6343 (2009).

[23] E. Moore and R. Tycko, Micron-scale magnetic resonance imaging of both liquids and solids, J. Magn. Reson. **260**, 1 (2015).

[24] E. O. Stejskal and J. E. Tanner, Spin diffusion measurements: Spin echoes in the presence of a time-dependent field gradient, J. Chem. Phys. **42**, 288 (1965).

[25] D. Le Bihan, Looking into the functional architecture of the brain with diffusion MRI, Nat. Rev. Neurosci. **4**, 469 (2003).

[26] D. S. Grebenkov, NMR survey of reflected Brownian motion, Rev. Mod. Phys. **79**, 1077 (2007).

[27] P. T. Callaghan, *Translational Dynamics and Magnetic Resonance: Principles of Pulsed Gradient Spin Echo NMR* (Oxford University Press, Oxford, 2011).

[28] J. Stepisnik, Time-dependent self-diffusion by NMR spin-echo, Phys. B **183**, 343 (1993).

[29] P. T. Callaghan and J. Stepisnik, Frequency-domain analysis of spin motion using modulated-gradient NMR, J. Magn. Reson. **117**, 118 (1995).

[30] N. Shemesh, G. A. Álvarez, and L. Frydman, Measuring small compartment dimensions by probing diffusion dynamics via non-uniform oscillating-gradient spin-echo (NOGSE) NMR, J. Magn. Reson. **237**, 49 (2013).

[31] I. Drobnjak, H. Zhang, A. Ianus, E. Kaden, and D. C. Alexander, PGSE, OGSE, and sensitivity to axon diameter in diffusion MRI: Insight from a simulation study, Magn. Reson. Med. **75**, 688 (2016).

[32] M. Nilsson, S. Lasic, I. Drobnjak, D. Topgaard, and C.-F. Westin, Resolution limit of cylinder diameter estimation by diffusion MRI: The impact of gradient waveform and orientation dispersion, NMR Biomed. **30**, e3711 (2017).

[33] H. H. Ong and F. W. Wehrli, Quantifying axon diameter and intra-cellular volume fraction in excised mouse spinal cord with q-space imaging, Neuroimage **51**, 1360 (2010).

[34] M. E. Komlosh, E. Ozarslan, M. J. Lizak, F. Horkay, V. Schram, N. Shemesh, Y. Cohen, and P. J. Basser, Pore diameter mapping using double pulsed-field gradient MRI and its validation using a novel glass capillary array phantom, J. Magn. Reson. **208**, 128 (2011).

[35] G. A. Álvarez, N. Shemesh, and L. Frydman, Coherent Dynamical Recoupling of Diffusion-Driven Decoherence in Magnetic Resonance, Phys. Rev. Lett. **111**, 080404 (2013).

[36] L. S. Kakkar, O. F. Bennett, B. Siow, S. Richardson, A. Ianus, T. Quick, D. Atkinson, J. B. Phillips, and I. Drobnjak, Low frequency oscillating gradient spin-echo sequences improve sensitivity to axon diameter: An experimental study in viable nerve tissue, Neuroimage **182**, 314 (2018), microstructural Imaging.

[37] J. Xu, X. Jiang, H. Li, L. R. Arlinghaus, E. T. McKinley, S. P. Devan, B. M. Hardy, J. Xie, H. Kang, A. B. Chakravarthy, and J. C. Gore, Magnetic resonance imaging of mean cell size in human breast tumors, Magn. Reson. Med. **83**, 2002 (2020). Epub 2019 Nov 25.

[38] J. Veraart, D. Nunes, U. Rudrapatna, E. Fieremans, D. K. Jones, D. S. Novikov, and N. Shemesh, Noninvasive quantification of axon radii using diffusion MRI, Elife **9**, e49855 (2020).

[39] J. Stepisnik, Validity limits of Gaussian approximation in cumulant expansion for diffusion attenuation of spin echo, Phys. B **270**, 110 (1999).

[40] J. Stepisnik, S. Lasic, A. Mohorix, I. Sersa, and A. Sepe, Spectral characterization of diffusion in porous media by the modulated gradient spin echo with CPMG sequence, J. Magn. Reson. **182**, 195 (2006).

[41] S. Lasic, J. Stepisnik, and A. Mohoric, Displacement power spectrum measurement by CPMG in constant gradient, J. Magn. Reson. **182**, 208 (2006).

[42] G. A. Álvarez and D. Suter, Measuring the Spectrum of Colored Noise by Dynamical Decoupling, Phys. Rev. Lett. **107**, 230501 (2011).

[43] A. Kofman and G. Kurizki, Acceleration of quantum decay processes by frequent observations, Nature **405**, 546 (2000).

[44] A. G. Kofman and G. Kurizki, Universal Dynamical Control of Quantum Mechanical Decay: Modulation of the Coupling to the Continuum, Phys. Rev. Lett. **87**, 270405 (2001).

[45] A. G. Kofman and G. Kurizki, Unified Theory of Dynamically Suppressed Qubit Decoherence in Thermal Baths, Phys. Rev. Lett. **93**, 130406 (2004).

[46] G. Gordon, N. Erez, and G. Kurizki, Universal dynamical decoherence control of noisy single- and multi-qubit systems, J. Phys. B: At. Mol. Opt. Phys. **40**, S75 (2007).

[47] G. Kurizki and A. Zwick, in *Advances in Chemical Physics* (John Wiley & Sons, Ltd, 2016), Chap. 4, Vol. 159, p. 137.

[48] A. Zwick, G. A. Álvarez, and G. Kurizki, Maximizing Information on the Environment by Dynamically Controlled Qubit Probes, Phys. Rev. Appl. **5**, 014007 (2016).

[49] J. R. Klauder and P. W. Anderson, Spectral diffusion decay in spin resonance experiments, Phys. Rev. **125**, 912 (1962).

[50] M. G. A. Paris, Quantum estimation for quantum technology, Int. J. Quantum Inf. **07**, 125 (2009).

[51] S. Braunstein and C. Caves, Statistical Distance and the Geometry of Quantum States, Phys. Rev. Lett. **72**, 3439 (1994).

[52] C. Benedetti and M. G. Paris, Characterization of classical gaussian processes using quantum probes, Phys. Lett. A **378**, 2495 (2014).

[53] G. Kurizki, E. Shahmoon, and A. Zwick, Thermal baths as quantum resources: More friends than foes? Phys. Scr. **90**, 128002 (2015).

[54] K. Setsompop *et al.*, Pushing the limits of in vivo diffusion MRI for the human connectome project, Neuroimage Mapping Connectome **80**, 220 (2013).

[55] S. Pajevic and P. J. Basser, An optimum principle predicts the distribution of axon diameters in normal white matter, PLoS ONE **8**, e54095 (2013).

[56] D. Liewald, R. Miller, N. Logothetis, H.-J. Wagner, and A. Schüz, Distribution of axon diameters in cortical white matter: An electron-microscopic study on three human brains and a macaque, Biol. Cybern. **108**, 541 (2014).

[57] M. Capiglioni, A. Zwick, P. Jimenez, and G. A. Álvarez, Non-invasive quantitative imaging of selective microstructure-sizes with magnetic resonance, arXiv:2006.02035 [physics.med-ph] (2020).